Second International Symposium on Marine Propulsors
smp'11, Hamburg, Germany, June 2011

# Propeller Loads of Large Commercial Vessels at Crash Stop

**J.W. Hur, H. Lee, B.J. Chang[1]**

[1]Hyundai Heavy Industries, Co., Ltd., Ulsan, Korea

## ABSTRACT

Propeller failure would occur at crash stop due to obscure reasons and become a dispute between propeller makers and ship owners. Hence, the study on the hydrodynamic propeller loads at crash stop is conducted in order to evaluate the structural safety of the propeller.

For the large commercial vessels, the torques of propeller shaft are measured at crash stop in the sea trial and compared with results of the Wageningen B-series charts and the commercial CFD code. The compared results show that the hydrodynamic loads are fluctuated at initial reverse rotation of the propeller but that the stresses on the blade at initial reverse rotation are lower than at maximum reverse rotation.

Based on these comparison results, the CFD methodology with the quasi-steady assumption is suggested to evaluate the structural safety of the propeller blade in initial design stage.

## Keywords

Propeller, Crash stop, CFD

## 1 INTRODUCTION

The crash stop astern is used to avoid navigating emergencies, such as collision and ground. During the astern condition, the propeller rotates reversely while ship still moves forward. In addition, hydrodynamic loads on propeller are changed dramatically due to the rapid change of propeller rotating direction. Hence, at crash stop astern, structural safety against the propeller failure could be significant.

During the crash stop astern, the direction of the inflow on the propeller blade is varied with change of the propeller RPM and the ship speed, as shown in Figure 1. From normal operation condition (A) to final astern condition (E) before ship stopping, the inflow direction is changed and the roles of leading edge and trailing edge are reversed. Furthermore, since the induced flow by the propeller is in opposite direction of the inflow, the large vortex ring is generated due to the strong interaction between both flows.

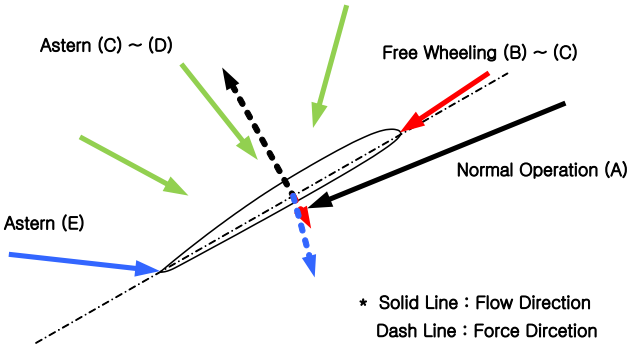


Figure 1: Inflow on blade section

To accurately predict hydrodynamic loads at crash stop condition, an expensive computation cost is required. Jang et al (2010) studied crash back of marine propulsors using Large Eddy Simulation (LES). Chang et al (2008) performed LES and structural analysis.

Black et al (2009) measured flow field during a crash back using particle image velocimetry. The propeller operated in the crash back range is tested, and in addition, structural analysis results are conducted. The maximum value at crash back is about 2 times higher than the mean root strain.

In general, the structural safety should be evaluated in the design stage, and therefore cheaper methodologies to analyze hydrodynamic loads are more applicable. Hence, in this study, although Reynolds-Averaged Navier Stokes equation (RANS) is not suitable to predict high fluctuated hydrodynamic loads especially in the large vortical flow, the procedures to evaluate the structural safety of the propeller blade at the crash stop, based on RANS, are suggested after studying the data measured in ship trials and comparing with results of Wageningen B-Series chart.

To understand the characteristics of the hydrodynamic loads at crash stop astern and to determine the calculation conditions for the CFD application, from data measured in sea trial, Fast Fourier Transform (FFT) and wavelet analysis are performed.

## 2 SUBJECT SHIP AND CRASH STOP SITUATION

First of all, 20,000 $m^3$ LPG Carrier is selected as the subject ship to understand the hydrodynamic characteristics at the crash stop. The main particulars of the subject ship are shown in Table 1.

| | | Ballast draft condition |
|---|---|---|
| Length between perpendiculars | [m] | 147.00 |
| Breadth | [m] | 25.50 |
| Draft (Fwd.) | [m] | 5.21 |
| Draft (Aft.) | [m] | 6.74 |
| Number | | 1 |
| Diameter | [m] | 5.7 |
| Number of blades | | 4 |
| Mean Pitch Ratio | | 0.7545 |
| Tip Skew | | 20.83 |
| Total Skew | | 24.50 |
| Direction of rotation | | RIGHT-HAND |
| Section type | | NACA |

Table 1: Main particulars of subject ship

The revolution of propeller is obtained by tachometer and the shaft torque is measured by a torque gauge with sampling rate 2.56 kHz. In parallel, ship speed is measured by speed log.

Figure 2 shows the fluctuation of the stress measured through torque gauge data on propeller shaft, according to the change of the revolution. Figure 3 shows change of the propeller revolution and ship speed synchronously.

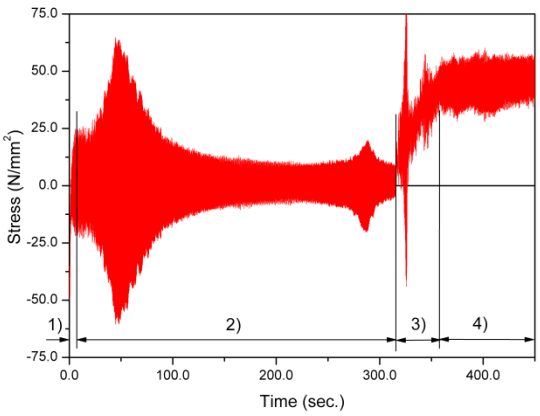


Figure 2: Measured stress data on propeller shaft

As shown in these figures, the ship is in transition state 1) as soon as the engine stops. Then, the free wheel state 2) continues for a while to avoid excessive loads on the shaft and engine. When engine RPM reaches below a critical level generally defined by the engine maker, the propeller starts reverse rotation and the revolution would be fluctuated in transition state 3). Then relatively constant revolution continues in full astern 4). In general, the durations of each state depend on engine power and ship size.

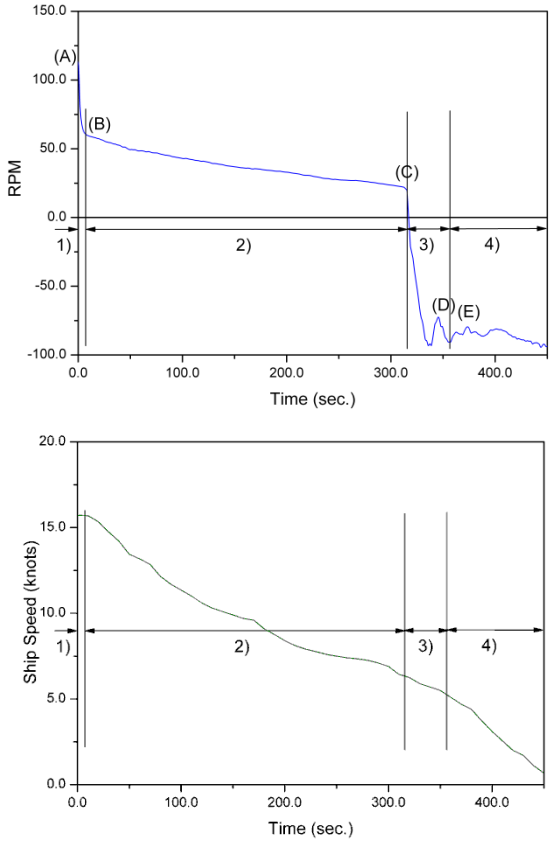


Figure 3: Measured astern RPM and ship speed

## 3 FREQUENCY ANALYSIS OF SEA TRIAL RESULTS

The characteristics of highly fluctuated stress measuring the torque shown in Figure 2 are studied using signal analysis techniques. First, FFT analysis is conducted on the data. As shown in Figure 4, the amplitude around 4 Hz is significant. To verify the change of above characteristics according to change of the state, the Morlet wavelet transformation is applied. As shown in Figure 5, the component around 4Hz is dominant around t = 50 and 320 sec., regardless of direction of propeller revolution, and this component is concluded to be independent on hydrodynamic loads. And the propeller revolution of each time is about 60 RPM and -60 RPM respectively. Thus, the vibration about 4Hz component is induced by structural vibration.

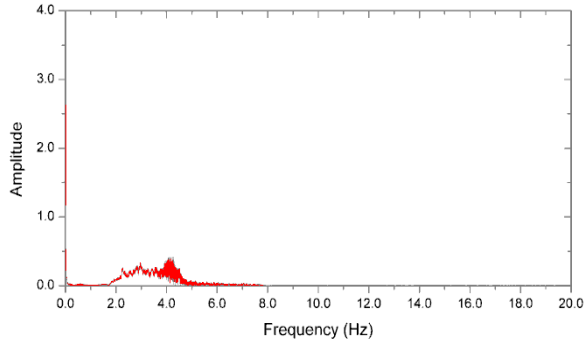


Figure 4: FFT result (amplitude spectrum) of stress data

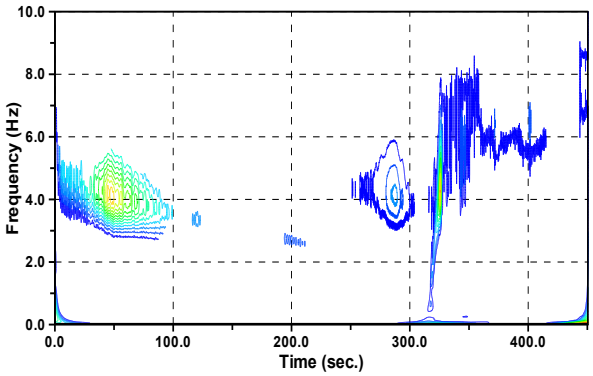


Figure 5: Wavelet analysis of stress data

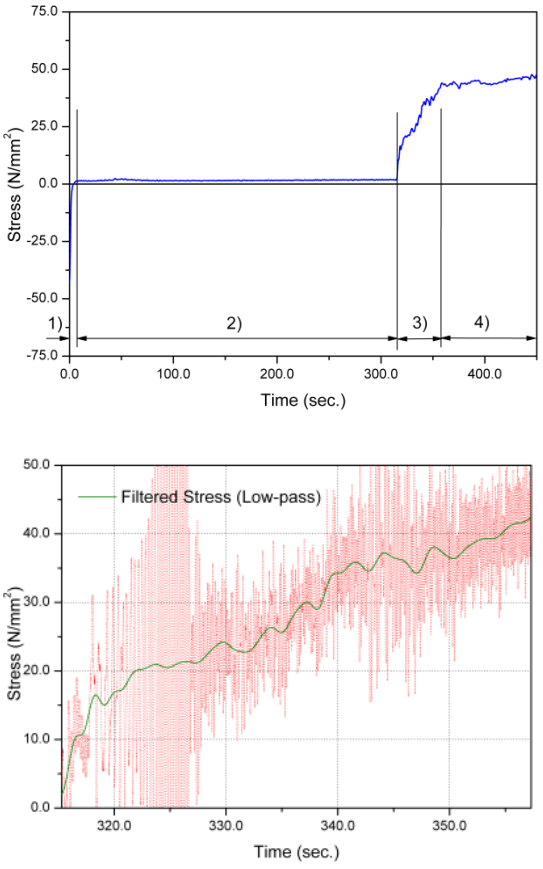


Figure 6: Filtered stress data (above : global, below : details at astern situation)

Based on above conclusion, the stress signal is filtered using low pass filter as shown in Figure 6, for comparison with analysis results. In this study, the stress during the transient state 3) is focused because the stress level is negligible during free wheel state and constant during the full astern state 4). For determination of analysis conditions, the ship speed and propeller revolution are also fitted using regression analysis, as shown in Figure 7.

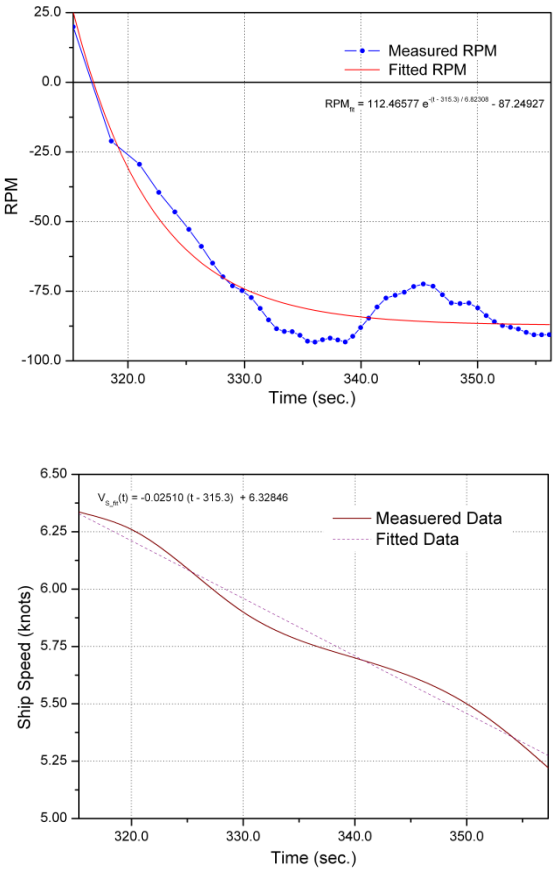


Figure 7: Fitted RPM and ship speed

## 4 ANALYSIS WITH WAGENINGEN B-SERIES CHART

As mentioned in the previous chapter, the purpose of this study is to set up the procedure of the structural safety assessment for the propeller at the crash stop. Hence, the applicability of existing series chart data is studied. For the propeller performance at 4-quadrant operating condition, Wageningen B-series chart is well published. This result is taken by interpolating B-series 4-quadrant chart data with EAR and P/D; and non-uniformity of inflows is not considered in using this series chart.

Based on the fitted ship speed and propeller revolution in Figure 7, the inflow angle on the propeller blade at 70% propeller radius is determined as shown in Figure 8. As the propeller begins to reverse revolution, the inflow angle is changed dramatically and becomes constant soon. The duration of angle change is shorter than that of Transient State 3).

In this approach, the effect of ship wake fraction is studied. The ship wake fraction is used from predicted value in towing tank tests. For more accurate results, the ship wake fraction needs to change according to the ship speed; but the used wake value 'w' is mean effective wake value at approach condition (w=0.315) without considering velocity distribution in this study. In Figure 9, the torque data taken by Wageningen B-series chart are shown and compared with the filtered torque converted from the stress measured in sea trial. From this comparison, the effect of ship wake is remarkable, and consideration of ship wake may give better agreement with measured data at initial transient states. However, this effect becomes small in the latter states. This result is regarded as an effect of the change of ship speed. At initial state, the ship speed is relatively high and the effect of ship wake is believed to be remarkable.

The difference of propeller blade shape and flow unsteadiness can be considered as reasons for the discrepancy between measured and predicted data. The propeller installed at the subject ship has relatively large skew in comparison with Wageningen B-series propeller. This effect of the blade skew may be remarkable especially at reverse rotation. As another reason, flow unsteadiness also is different between sea trial and series chart tests. The flow around the propeller is highly fluctuated and has unsteady characteristics during the crash stop in sea trial. But the prediction with series chart is performed with steady inflow. Despite this discrepancy, the series charts give relatively high torque values, marginal in evaluation of structural safety.

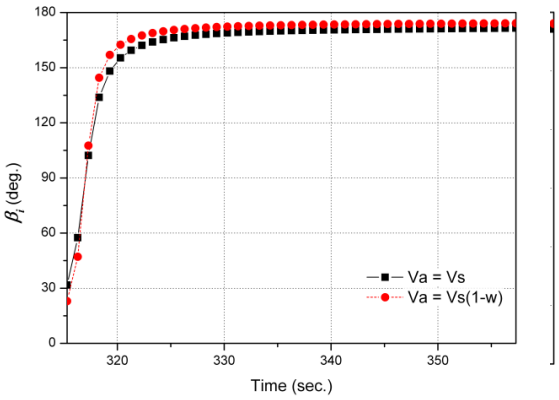


Figure 8: Inflow angle for transient state

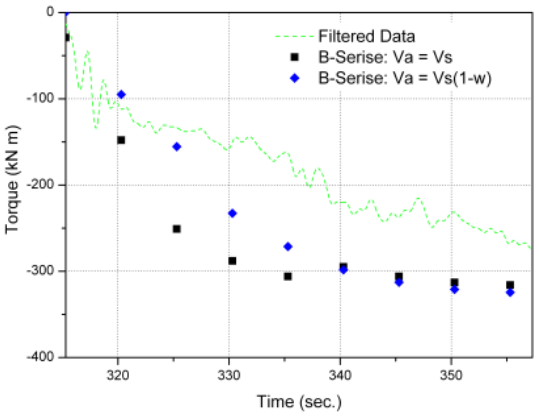


Figure 9: The torque data taken by Wageningen B-series

## 5 CFD SIMULATIONS

As mentioned in the introduction, the flow around propeller at the crash astern situation is highly unsteady due to interaction between the inflow and flow induced by propeller action. Also, ship speed and propeller revolution vary with time. Therefore, in applying CFD, transient methodologies in combination with computationally heavy turbulence, models like LES are required; and a large computation domain including the ship may give us realistic results. However, so far, the computational costs of these approaches are too expensive to be frequently used in design stages.

Fortunately, prediction using the series chart data agrees well with the measured data in acceptable tolerance for structural safety. Also, recently, RANS solver is used widely in predicting propeller performance, due to the advantage of computing power. Krasilnikov et al (2009) and Müller (2009) predict propeller open water performance using Moving Reference Frame (MRF).

Therefore, in this paper, usefulness of RANS approaches assuming uniform inflow is studied for the propeller in the crash stop situation.

### 5.1 Numerical Method

The commercial solver Star-CCM+ is used for numerical simulation. It supports unstructured mesh generation and RANS solver. The governing equations of the method to be solved are below:

$$\frac{\partial U_i}{\partial x_i} = 0 \qquad (1)$$

$$\frac{\partial U_i}{\partial t} + U_l \frac{\partial U_i}{\partial x_l} = -\frac{\partial p}{\partial x_i} + \frac{\partial}{\partial x_l}\left(\frac{1}{R_N}\frac{\partial U_i}{\partial x_l} - \overline{u_i u_l}\right) \qquad (2)$$

where $U_i$ is velocity vector; p = pressure; $R_N$ = Reynolds number; $-\overline{u_i u_l}$ = Reynolds stresses. Reynolds stresses are determined from turbulence model. For turbulence modeling, Spalart-Allmaras model based on single transport equation is used.

### 5.2 Grid and Boundary Conditions

Computational domain and boundary conditions are shown in Figure 10. The computational domain has (360 degrees)/(number of blade) section, due to the periodicity in the circumferential direction. It is consisted of the propeller and shaft. Assuming that operation condition is the uniform inflow, numerical simulation is conducted in MRF model. The computational domain was defined of propeller diameter D. The computational domain regions are: the length of inlet and outlet region 7.5D, radius of domain 5D.

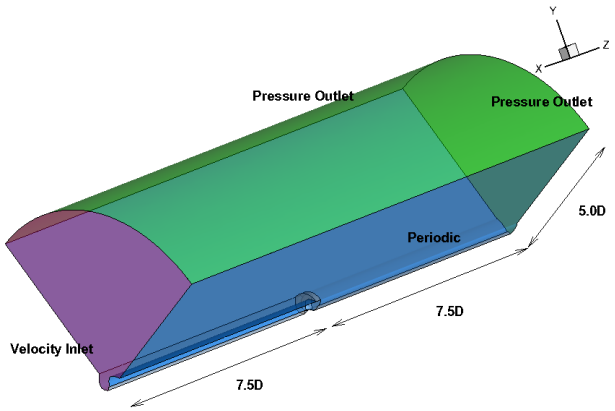


Figure 10: Computational domain and boundary conditions

Velocity inlet boundary condition is specified in front of propeller. At radial and lateral direction, pressure outlet boundary condition is specified. Periodic boundary condition is specified at circumferential direction. Computational grid for simulation is meshed by polyhedral. For more accurate solutions, prism mesh is adopted to grid at surface of propeller. Surface mesh pattern is shown in Figure 11. The size of domain and mesh fineness is determined after checking the effect on the simulated results. Table 2 shows information of grid.

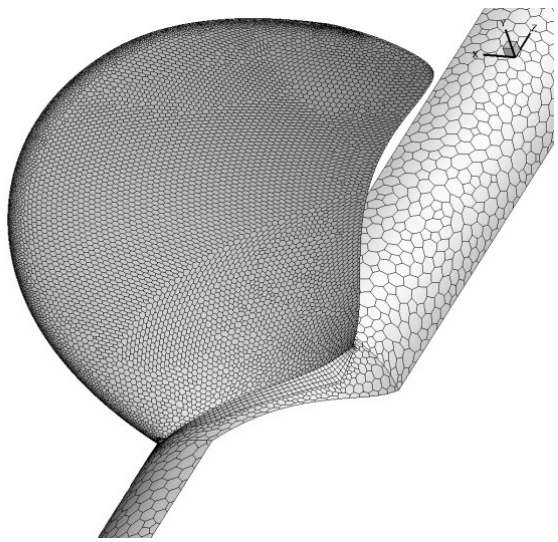

Figure 11: Computational grid for CFD calculation

| | |
|---|---|
| Number of mesh at Blade part | 139,545 |
| Number of mesh at Domain part | 118,118 |
| Total Number of mesh | 257,663 |
| Min. grid spacing | 0.001 D |

Table 2 Information of computation grid

### 5.3 Results

The analysis of propeller open water test is performed for subject propeller. The difference between calculated $K_T$, $K_Q$ and model test results is slightly in the overall rage of the advance ratio as shown at Figure 12.

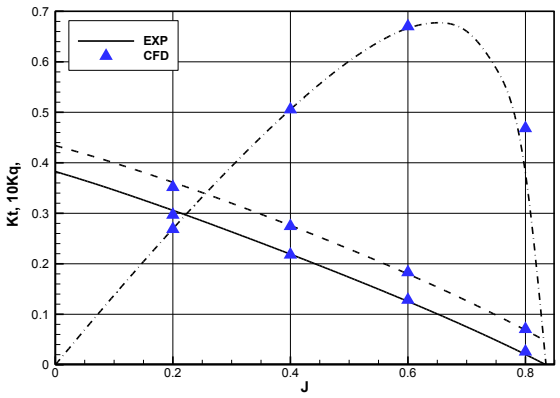


Figure 12 Propeller Open Test

The crash stop astern simulation is conducted in 2 ways. One is steady analysis, another is unsteady (transient) analysis. Through filtering the sea trial results, the operating conditions are determined for the propeller RPM and ship speed, which is specified to be a function of time in transient analysis. For each analysis, the effect of ship wake fraction is studied like series chart application. The calculated torque is compared with the measured torque in Figure 13 and the corresponding thrust is shown in Figure 14.

After propeller started to reverse, torque of propeller has peak point about 5-10 sec later. The torque of propeller is gradually increased and is seem to reach at full astern. The effect of ship wake fraction is remarkable even in the latter state as well as the initial state. In initial state, consideration of ship wake fraction relatively agrees well with the measured data, but shows large discrepancy at the latter state. It is due to the change of ship speed as mentioned in previous chapter. Steady analysis does not represent the detailed peak level of torque, but overall trend of the steady analysis is similar to that of transient analysis.

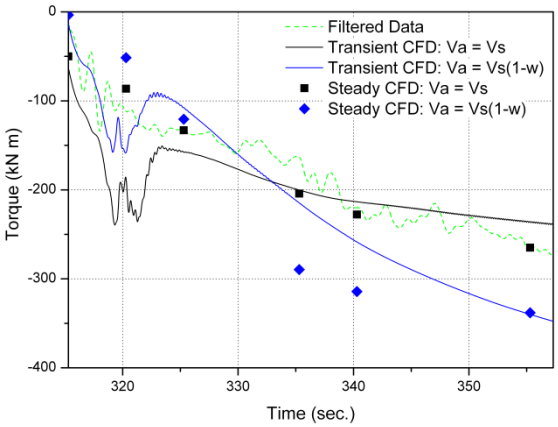


Figure 13: Torque data taken by CFD

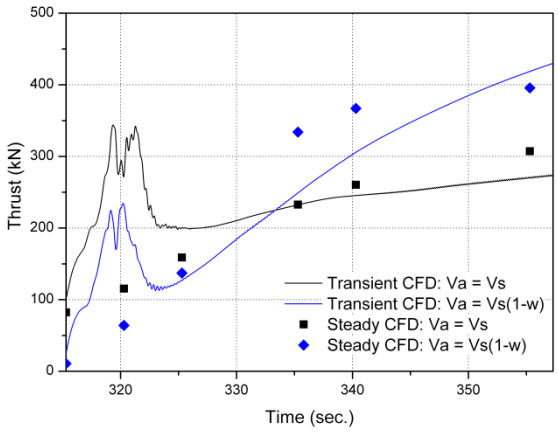


Figure 14: Thrust data taken by CFD

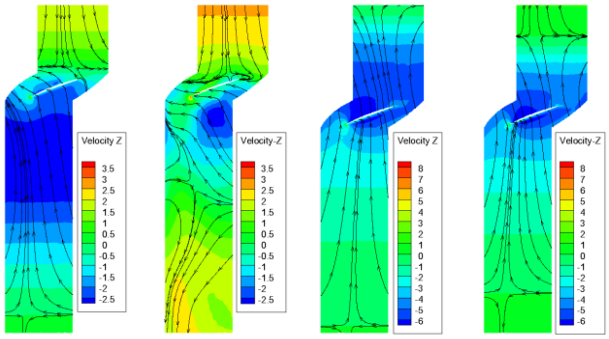

(a) (b) (c) (d)

Figure 15: Stream line and axial velocity contour at 0.7 r/R (t=315.3 + 5 sec.: (a) steady, (b) transient, t=315.3 +40 sec.: (c) steady, (d) transient)

To verify the discrepancy between steady and transient analysis, the flow patterns around blade are compared. Figure 15 shows the stream line around the propeller blade at 0.7r/R at initial reverse rotation and full astern of the propeller. As mentioned in the introduction, the difference of direction between inflow and induced flow makes large vortex ring including propeller. The vortex ring is simulated at each methodology but the size of vortex, which is affect the torque of propeller, is different according to analysis methodology.

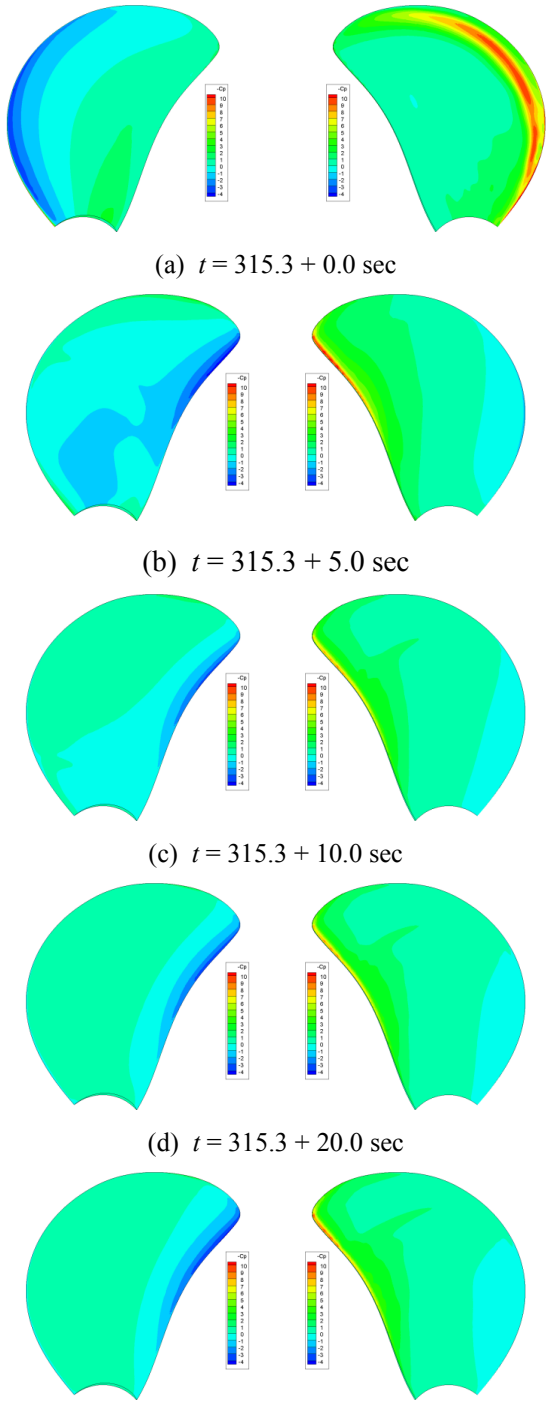

(a) $t$ = 315.3 + 0.0 sec

(b) $t$ = 315.3 + 5.0 sec

(c) $t$ = 315.3 + 10.0 sec

(d) $t$ = 315.3 + 20.0 sec

(e) $t$ = 315.3 + 40.0 sec

Figure 16: -Cp for steady condition (left: back side, right: face side)

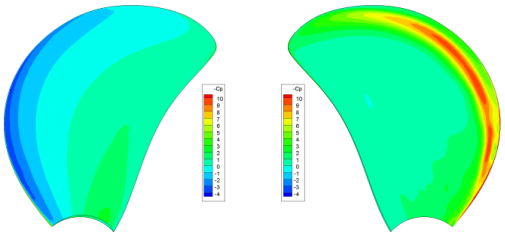

(a) $t$ = 315.3 + 0.0 sec

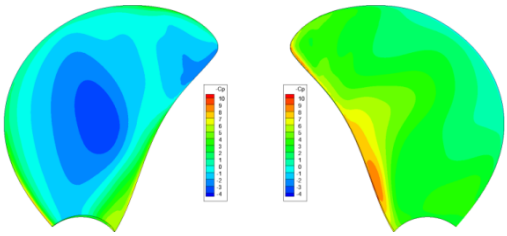

(b) $t$ = 315.3 + 5.0 sec

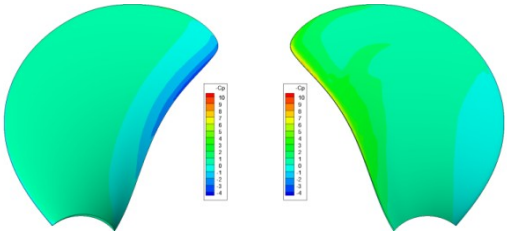

(c) $t$ = 315.3 + 40.0 sec

Figure 17: -Cp for transient condition (left: back side, right: face side)

As mentioned above, the stream line at 0.7r/R shows the effect of magnitude of simulated vortex. The magnitude of simulated vortex for steady analysis is larger than that of transient analysis. These differences of vortex magnitude affect the stream line around the propeller and change the propeller angle of attack as shown in Figures 15 (a) and (b). By comparing the results of sea trial and analysis, steady analysis seems to be under-predicted at initial reverse rotation of the propeller. Figure 15 (c) and (d) show the stream line around the propeller blade at 0.7r/R at full astern. The difference of the magnitude of simulated vortex between steady and transient analysis is smaller than initial reverse rotation because the vortex for steady and transient analysis is fully developed at full astern condition. Thus, the difference of the propeller angle of attack between steady and transient analysis at full astern condition is slight. As per these results, the steady analysis is efficient and gives good agreement for full astern, while the transient analysis is consumed large computing time.

Pressure distributions on blade surface of steady and transient analysis are shown in Figures 16 and 17. Figures 16 and 17 show that the role of leading edge and trailing edge are exchanged. It can be seen the -Cp difference between steady and transient analysis at 315.3 + 5.0 sec, which is at initial reverse rotation of the propeller. On the other hand, pressure distributions of steady and transient analysis are similar at 315.3 + 40.0 sec, which is full astern condition, as like stream line.

Structural analysis can be performed by using these results. Since hydrodynamic loads on propeller blade at full astern condition are higher than the loads at initial reverse rotation, the numerical simulation at full astern condition is significant in the point of view of structural analysis. For these reasons, the steady analysis at full astern is more appropriate to the evaluation of structural analysis.

## 6 CONCLUSIONS

In this study, the prediction of loads on the propeller at crash stop is performed in order to evaluate the structural safety of the propeller. The prediction is conducted by using Wageningen B-series chart and CFD. To determine operation conditions for crash stop, the sea trial result is analyzed by FFT and wavelet analysis. From these results, the ship speed and propeller RPM are also modeled by using regression analysis for operation conditions.

The prediction which uses the Wageningen B-series chart data corresponds with the measured data at an acceptable level for structural safety, in spite of the difference of propeller blade shape and flow steadiness. But structural evaluation cannot be performed by the results of series chart since this application cannot predict the distribution of pressure on the propeller blade.

Hence, CFD is used for the prediction of the loads acting on the propeller. The numerical simulation is performed at the crash stop through RANS solver for steady and transient analysis. It can be seen that the difference between steady and transient simulation is large at initial reverse rotation, but it is reduced at full astern condition. In regard to this characteristic, the steady analysis cannot simulate the detailed peak level of torque, but transient analysis can. Since the stresses on the propeller blade at the full astern condition are higher than at initial reverse rotation, numerical simulation at full astern is significant in structural analysis. The steady analysis at full astern is more useful methodology than transient analysis, because consumed computing time for steady analysis is shorter than transient analysis.

The results of the simulation for both steady and transient analyses at full astern are in good agreement with the sea trial results. Through comparing sea trial results and CFD results, it is suggested to evaluate the structural analysis of the propeller at initial design stage with the steady analysis at full astern condition.

## REFERENCES

Black, S. & Swithenbank, S. (2009). 'Analysis of Crashback Forces Compared with Experimental Results'. First International Symposium on Marine Propulsors, Trondheim, Norway.

Chang, P. A., Ebert, M., Young, Y.L., Liu, Z., Mahesh, K., Jang, H. & Shearer, M. (2008). 'Propeller Forces and Structural Response due to Crashback'. 27th Symposium on Naval Hydrodynamic, Seoul, Korea.

Daubechies, I. (1988). 'Orthonormal bases of compactly supported wavelets'. Commun. on Pure and Appl. Math. **41**, pp. 909-996.

IMO. (2002). 'Standard for Ship Manoeuvrability'. IMO Resolution MSC **137**(76).

Jang, H. & Mahesh, K. (2010). 'Large Eddy Simulation of Marine Propulsors in Crashback'. 28th Symposium on Naval Hydrodynamic, Pasadena, California.

Krasilnikov, V., Sun, J. & Halse, K. H. (2009). 'CFD investigation in scale effect on propellers with different magnitude of skew in turbulent flow'. First international symposium on marine propulsors, Trondheim, Norway.

Müller, S-B., Moustafa, A-M. & Hibert, G. (2009). 'Scale effects on propellers for large container vessels'. First international symposium on marine propulsors, Trondheim, Norway.

Newland, D. E. (1993). An introduction to random vibrations, spectral & wavelet analysis. Addison Wesley Longman Limited.